Article

Experimental Investigation on Toughness of SFRC and Bond Behavior with Reinforcing Bars

Hongmei Zhang [1], Zizhao Tang [1], Jinguang Li [2], Zheming Hu [1] and Qian Feng [1,*]

1 College of Civil Engineering and Architecture, Zhejiang University, Hangzhou 310058, China; zhanghongmei@zju.edu.cn (H.Z.); 22112277@zju.edu.cn (Z.T.); 3180104574@zju.edu.cn (Z.H.)
2 Hunan Track Survey and Design Co., Ltd., Changsha 410020, China; lijinguang_chsh@163.com
* Correspondence: fengqian@zju.edu.cn

Abstract: Steel-fiber reinforced concrete (SFRC) has the advantages of high strength, durability, and crack prevention ability. Studies on the compressive strength, tensile strength and flexural behavior of SFRC have been carried out by many researchers. In this paper, the toughness of SFRC along with the bond behavior between SFRC and reinforcement were investigated. Hooked-end and straight steel fibers were chosen in the toughness tests of SFRC. The test results show that the SFRC mixtures with hooked-end steel fibers exhibit higher toughness. In addition, hooked-end steel fibers were chosen to be mixed in the SFRC to demonstrate the bond behavior between SFRC and reinforcing bars. Different embedment lengths were considered in the tests to show the influence of the anchorage area on the bond–slip responses in the pull-out tests. The failure modes for different specimens were exhibited. The results show that the embedment length more than 5 times the bar diameter causes tensile failure of the reinforcement, while the embedment length of 3 times the bar diameter causes pull-out failure of the reinforcement.

Keywords: SFRC (steel-fiber reinforced concrete); toughness; reinforcement; bond; embedment length

1. Introduction

Steel-fiber reinforced concrete (SFRC) is a cementitious composite through an appropriate combination of cement, coarse aggregates, fine aggregates and randomly distributed short steel fibers [1]. Compared with normal strength concrete (NSC), the SFRC possesses higher compressive strength, tensile strength, and greater durability [2]. Because of its superior quality, the SFRC has been widely used in engineering projects including the aspects of flooring [3,4], tunnels [5], pipe fittings [6], bridges [7,8], roads [9], etc. Research work [10–13] shows that adding steel fibers to different kinds of concrete can improve its toughness and reduce cracking. When it comes to high-strength concrete, adding steel fibers serves two purposes: preventing cracks from forming and improving toughness. Meanwhile, high-strength concrete can be brittle, which is where the addition of steel fibers becomes beneficial. By combining the benefits of both materials, SFRC exhibits better strength and toughness behavior.

Researchers have utilized SFRC to improve the performance of structural components due to its advantages [14–17]. Researchers discovered that the addition of steel fibers in cementitious composites delayed cracking and damage processes in shear walls, leading to decreased damage extent over time. The two typical shapes of steel fibers are straight steel fibers (SFs) and hooked-end steel fibers (HFs). Studies have been focused on their compressive strength and flexural behavior [18–21]. Kotatkova et al. [18] compared different

types of steel fibers (straight and hooked-end) in relation to their influence on the final mechanical properties of high strength concrete (HSC) and reported the better performance of hooked-end steel fiber. Wu et al. [19] carried out corresponding tests and concluded that compared with corrugated and straight fibers, the hooked-end fibers provided better performance in improving the compressive and flexural strength of concrete. Kim et al. [20] conducted a pull-out experiment to investigate the bond performance of the two types of steel fibers in SFRC. As a result, they found that UHPC mixtures with hooked-end steel fibers exhibit higher bonding strength than that of straight steel fibers. Shaikh et al. [21] discussed the pullout load–displacement behavior of hook end steel fibers having double, triple, and quadruple bends in their ends in geopolymers and cement mortars. This paper investigates the effects of two types of steel fibers on the compressive and flexural strength, as well as the compression toughness and bending toughness of high-performance concrete reinforced with eco-friendly material slag powder.

The toughness of SFRC influences the structural behavior of the structural members, including the capacity to consume energy, the bond–slip characteristics, failure modes and tension stiffening of reinforced concrete, which would further influence the structural durability and security. Theoretically, with the bridging action provided by the steel fibers, the confinement effect on the reinforcement from the cementitious composites would strengthen the bond between reinforcement and SFRC. Meanwhile, the bond–slip behavior between the reinforcement and concrete provides very important information to evaluate the structural capacity, which would further influence the structural durability and security. Numerous researchers have studied the pull-out characteristics of reinforcement in steel fiber concrete.

Research work [22–24] shows that the pull-out failure mode can be influenced by parameters including concrete strength, the ratio of concrete cover to reinforcement diameter (c/d), embedment length of reinforcement, yielding strength of reinforcement and so on for normal reinforced concrete. Researchers have also studied the bond–slip behavior in SFRC. Dancygier et al. [25] investigated the effect of concrete strength and steel fibers on bond strength, as well as the effect of reinforcement dimensional properties and concrete cover, thus presenting an empirical expression representing the coupling of these effects. Chao et al. [26] studied the effect of strain-softening and strain-hardening fiber-reinforced cementitious (FRC) composites on the bond strength and bond stress–slip response of deformed steel reinforcing bars, showing that the bridging effect provided by the fibers in FRC composites after cracking can effectively provide post-cracking tensile resistance to the concrete matrix and limit the crack width. Sarraz et al. [27] proposed a numerical method based on a 3D rigid-body spring model to evaluate the bonding behavior of deformed bars in fiber-reinforced cementitious composites and found that discrete fibers were the main factor preventing the propagation of split bond cracks, and stress propagation indicated the presence of high local bond stresses around the rebar, which improved the bond ductility. Hameed et al. [28] conducted the pull-out tests using amorphous metal fibers and carbon steel hook-end fibers to evaluate the application of metal fibers to confine the concrete in column-beam joints, showing that both types of fibers helped to improve the peak bond stresses and also the stiffness of the rising branch in the bond slip curve. Yazıcı et al. [29] studied the impact of the concrete cover and the number of steel fibers on bond between reinforcing bars and the SFRC. It turns out that the increase in the quantity and aspect ratio of steel fibers in the SFRC enhances the pull-out load. Soroushian et al. [30] investigated the impact of steel fiber on the local bond behavior between the deformed reinforcement and the constrained concrete. They discovered that the slip corresponding to the peak bond stress decreased with the existence of fibers. According to Yan et al. [31], the addition of

steel fibers can significantly enhance both the bonding performance between concrete and reinforcement and the concrete's own resistance to crack development.

Although there have been many studies about the interaction between reinforcement and SFRC [25–34], there have been even fewer studies investigating embedment length influences on the global load–slip response from the partial-interaction pull-out tests of reinforcement from SFRC. To further explore the bond characteristics between SFRC and reinforcement, an experimental investigation was carried out to analyze the difference in this type of bond caused by the different embedment length of reinforcement and SFRC and also with the comparison group of reinforcement embedded in normal concrete. The load–slip responses were obtained. Also, the data points in each load–slip curve were collected and processed. Important parameters such as concrete cover, reinforcing bar diameter and other material properties of reinforcement along with SFRC were considered. The failure modes for each specimen are explored in detail and the reasons for this are described in this paper.

2. Toughness Test of SFRC

The toughness test of SFRC consists of a compressive toughness test and a bending toughness test. The test specimens, procedures and results are as follows.

2.1. Test Specimens

The mixture proportion of concrete is described in Table 1. The experiment used P.II 52.5 Portland cement; coarse aggregate consisted of crushed basalt stones with a maximum size of 1 cm; fine aggregate was medium sand with a fineness modulus of 2.6 and grading zone II; the slag powder used was S95 grade. Two types of steel fibers were employed to produce SFRC. Figure 1 shows the straight steel fibers (SFs) and hooked-end steel fibers (HFs) investigated in this study. The straight fibers were 0.2 mm in diameter and 12 mm in length, of which the tensile strength was no less than 3000 MPa. The hooked-end fibers were 0.4 mm in diameter and 32 mm in length, with tensile strength no less than 1700 MPa. The fiber content was 0% for steel fibers in the group of specimens named 'H0', 1.5% for the SF in specimens named 'H15-S', and 1.5% in 'H15-H' to investigate the effect of different fiber types on the SFRC properties.

Table 1. Mixture proportion of concrete (kg/m^3).

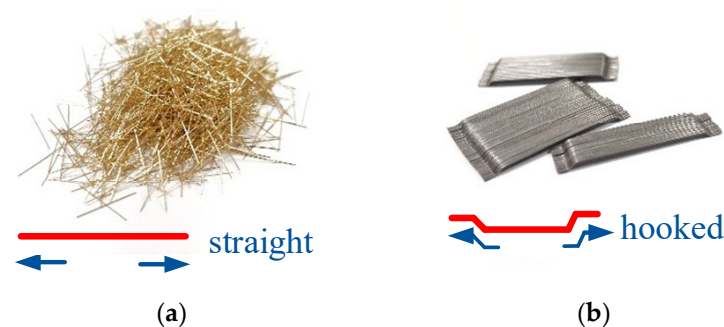| Specimens	Cement	Slag Powder	Coarse Aggregate	Fine Aggregate	Water	Admixture	Steel Fiber
H0	411	50	410	1026	250	3	0
H15-S	411	50	410	1026	250	4	118 (SF)
H15-H	411	50	410	1026	250	4	118 (HF)

Figure 1. Different types of steel fibers. (**a**) Straight steel fibers. (**b**) Hooked-end steel fibers.

The tests were carried out to obtain the compressive strength of concrete by using cubes with a side length of 150 mm. Each group includes four specimens. The compressive strength of the concrete cube, the mean value of the prismatic compressive strength, the strain corresponding to the peak stress and the elastic modulus of the proportioned concrete in each group are shown in Table 2.

Table 2. Material properties of the proportioned concrete.

Specimens	Cubic Strength (MPa)	Prismatic Strength (MPa)	Peak Strain (10^{-6})	Elastic Modulus (10^4 MPa)
H0	74.2	67.5	2526	3.749
H15-S	70.5	63.3	3019	3.714
H15-H	71.1	63.7	2989	3.720

2.2. Test Procedures for the Compression Toughness

The compressive toughness was investigated using prismatic specimens with the size of $100 \times 100 \times 300$ mm and 4 specimens per group. An INSTRON-8805 electro-hydraulic servo fatigue testing machine was used for loading. An NCS YYU-5/50 extensometer was used for the strain measuring, which was installed in the middle of the specimen. The test was performed under a constant displacement rate of 0.2 mm/min.

The failure modes of the three types of specimens H0, H15-S and H15-H are shown in Figure 2b–d. The normal concrete specimens of H0 collapsed into large fragments along the main crack. Then, the specimen was furtherly destroyed into several pieces under the compression load. The failure surface was basically parallel to the loading direction. A smoother stone section was observed on the failure surface, which indicated that the crack directly penetrated through the coarse aggregate and caused the final failure. However, the specimens of H15-S and H15-H still maintain a good integrity after damage, showing a multi-crack damage pattern. This phenomenon could be attributed to the bridging effect provided by the steel fibers.
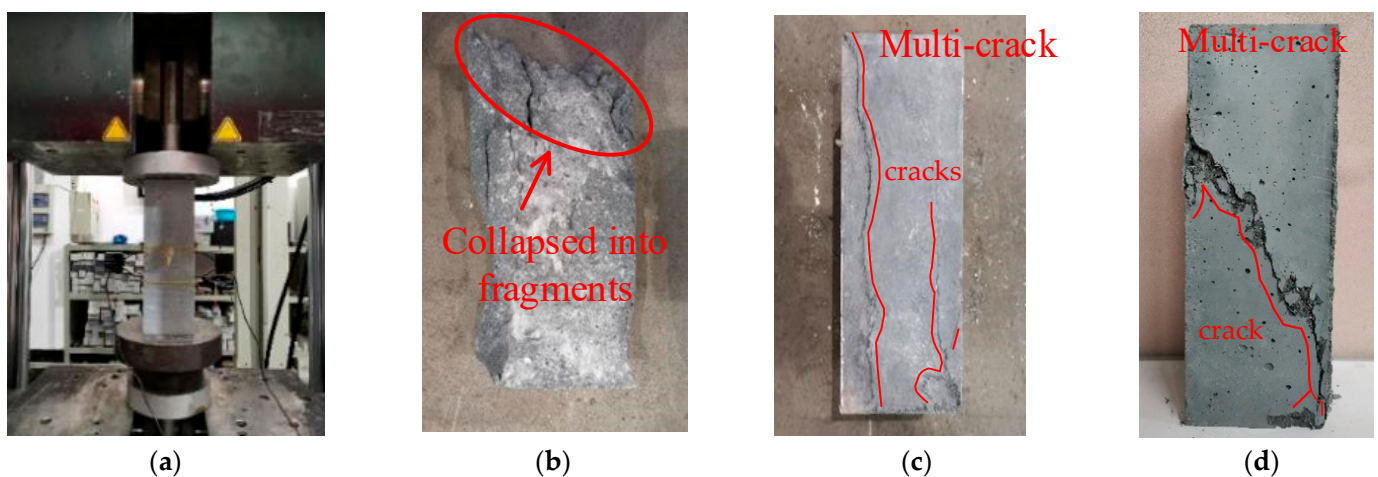

Figure 2. Test setup and failure models of specimens. (**a**) INSTRON-8805. (**b**) Specimen: H0. (**c**) Specimen: H15-S. (**d**) Specimen: H15-H.

The steel fibers at the crack can transfer the stress to the concrete through the surface, resulting in a slower crack expansion by connecting the two concrete surfaces. It also extends the damage process of the specimen. In the later stages of loading, several short cracks appeared on the surface of the H15-H specimen in the diagonal direction along the

side, and as the steel fibers were gradually pulled out, the cracks developed slowly with the loading. Then, the cracks eventually connected to form a damage zone. The angle formed by the crack direction and the loading direction in the specimen H15-S were much less than that of the specimen H15-H.

The CT scan was conducted to investigate the microscopic failure mechanism of the specimens and Figure 3a,b show the matrix and coarse aggregate interface in the failed specimen. The microcracks of the concrete and spalling of the cement matrix were observed near the fiber hole grooves in Figure 3c,d, which indicates that the interfacial transition zone of steel fibers and cementitious substrate was the weak area and was more prone to damage. The debonding of steel fiber and the matrix is shown in Figure 3e.
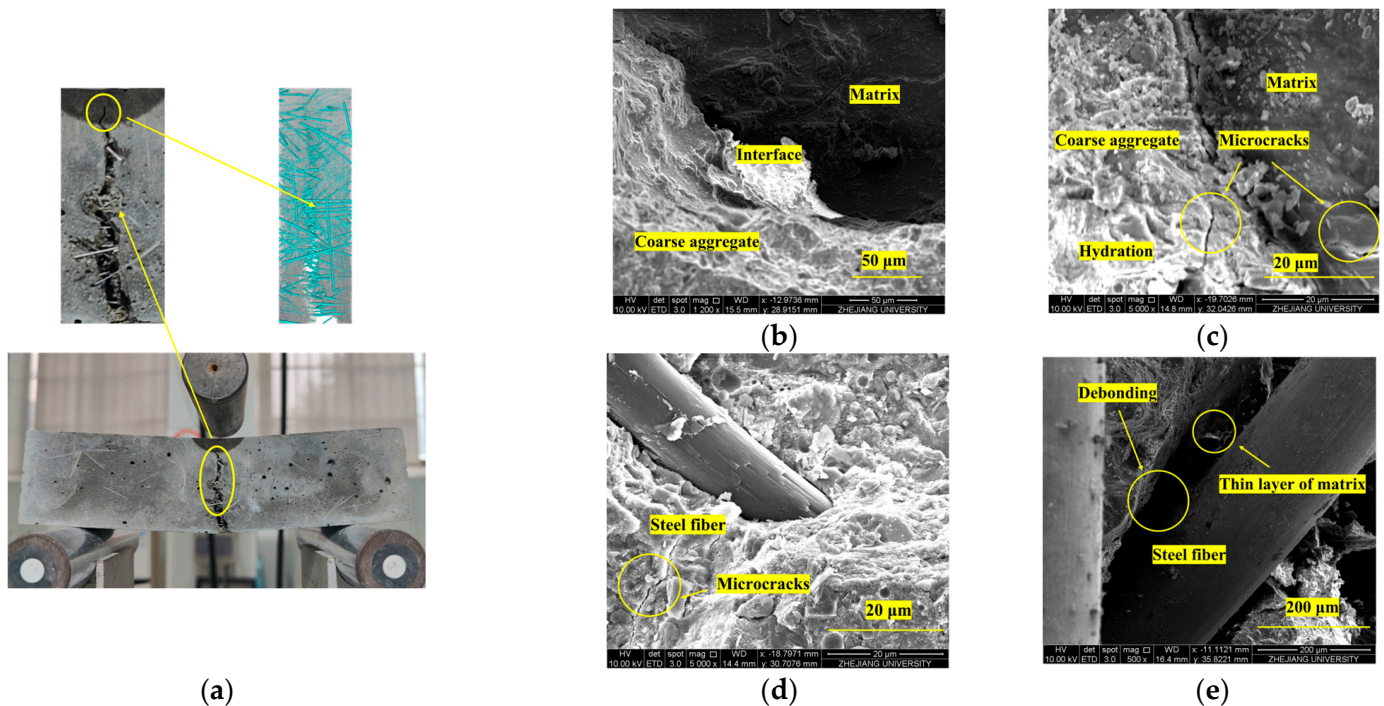

Figure 3. CT scan of SFRC. (**a**) The scan area. (**b**) The matrix and coarse aggregate interface. (**c**) Internal microcracks. (**d**) Steel fiber. (**e**) Debonding of steel fiber and matrix.

Figure 4a plots the averaged stress–strain curves of the SFRC with different fiber contents. After reaching the ultimate strength, there was a significant dramatic drop for H0. Meanwhile, compared with H0, the H15-S and H15-H showed a milder descending slope compared with H0, which indicates that adding steel fibers improves the ultimate strain of UHPC mixtures. When the compressive stress drops to 85% of its peak value, the strain for H15-H is 1.84 times that of H0 and 1.26 times that of H15-S. Furthermore, at the strain value of 0.030, H15-H maintained 30% of the peak stress, which demonstrates its ductile behavior. Figure 4 shows that there is no obvious difference in the compressive strength between SFRC H15-S/H15-H and the concrete without fibers H0. Because of the addition of the steel fibers, weak interfaces were created, causing the development of cracks in the loading process. The strengthening effect of the steel fibers coexisted with the weakening of the concrete strength by the weak interfaces, which leads to the unobvious effect of steel fibers on the compressive strength.
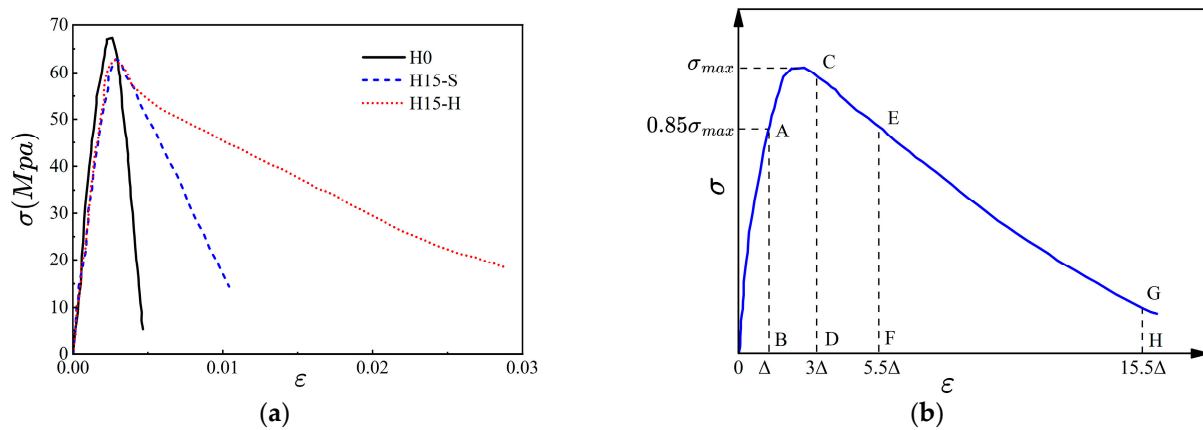
Figure 4. Stress–strain properties. (**a**) Compressive stress–strain relationship of concrete. (**b**) Schematic diagram of concrete toughness index.

The toughness of SFRC is commonly determined by using several different methods [17]. A clear definition of the compressive toughness index is given according to Chinese CECS13:89 [16]. In this study, the compressive toughness of SFRC is quantified by the toughness index η_{c5}, η_{c10} and η_{c30}. As shown in Figure 4b, the three toughness indices are calculated as (1) $\eta_{c5} = S_{OACD}/S_{OAB}$; (2) $\eta_{c10} = S_{OAEF}/S_{OAB}$; and (3) $\eta c30 = S_{OAGH}/S_{OAB}$, where S is the area enclosed by the subscripts.

Table 3 lists the calculated results of the toughness index. As shown in Figure 4, the strengthening for the compressive resistance from the steel fiber on SFRC was mainly exhibited on the descending branch of the stress–strain relationship. In terms of η_{c10}, H0 had no compressive toughness compared with H15-S and H15-H while the values for H15-S and H15-H are close. In terms of η_{c30}, straight fiber mixtures showed very low toughness, while hooked-end fibers mixtures showed great toughness performance. In conclusion, the compression toughness of steel fiber concrete H15-S and H15-H are greater than that of the normal concrete H0, while the hooked-end steel fiber concrete H15-H shows the best compression toughness among the three types of specimens.

Table 3. Toughness index of concrete.

Specimens	η_{c5}	η_{c10}	η_{c30}
H0	3.57	-	-
H15-S	3.86	5.64	-
H15-H	3.76	6.54	14.12

2.3. Test Procedures for the Flexural Toughness

The flexural toughness of SFRC was investigated by using prismatic specimens with the size of 100 mm × 100 mm × 400 mm. Each specimen was subjected to the fourth-point loading. There are four specimens per group. The INSTRON-8805 electro-hydraulic servo fatigue tester was used as the loading device and a MILONT-F10 displacement meter was used to measure the deflection of the specimen in the middle span.

The experimental results are shown in Table 4. The peak values of the flexural stress of the concrete were increased considerably due to the adding of steel fibers. The specimen type of H15-S containing hooked-end fibers provided the largest value of flexural strength, which was 13.74 MPa. Figure 5b shows that the load–deflection curve of H0 broke down shortly after the peak value showing an obvious steep drop tendency, while H15-S and H15-H exhibited a relatively slow drop, which indicated that the type of H0 shows more brittle ductile behavior than the other two types of specimens.
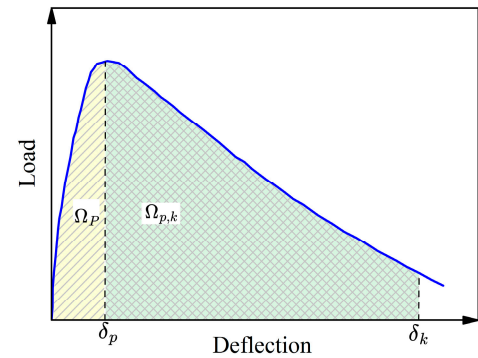
Table 4. Experimental tensile results of concrete.

Specimens	Peak Load (kN)	Tensile Strength (MPa)	Mid-Span Deflection (mm)
H0	19.49	7.78	0.35
H15-S	34.72	13.74	1.46
H15-H	33.24	13.08	1.42
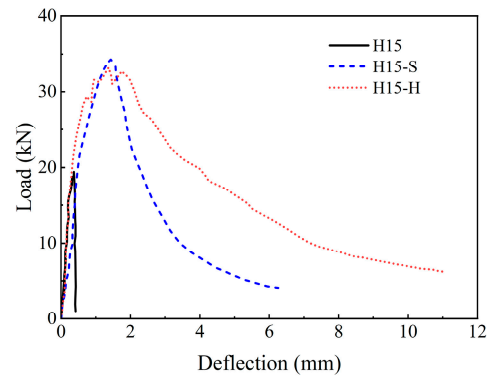
Figure 5. Test setup for flexural toughness and test results. (**a**) Flexural toughness test. (**b**) Flexural load–deflection curves. (**c**) Flexural toughness ratio calculating diagram.

Test methods have been developed to evaluate flexural toughness [35]. However, existing methods are relatively simple in determining the initial cracking point, which could lead to a larger deviation made by humans in determining the flexural toughness index. Gao [36] proposed an improved evaluation method, using the initial flexural toughness ratio and the residual flexural toughness ratio to avoid the determination of the initial cracking point. Figure 5c shows the calculation method of flexural toughness, where δ_p refers to the mid-span deflection corresponding to the peak load and δ_k refers to the given mid-span deflection.

Table 5 shows the calculation results for the flexural toughness ratio according to Gao's method. Adding straight fibers and hooked-end fibers improved the initial flexural strengths of SFRC by 90% and 144%, respectively. The initial flexural toughness of SFRC was also significantly improved. H15-H exhibited the best toughness performance among these three types of mixtures.

Table 5. Calculation results of flexural toughness ratio of concrete.

Items	$f_{e,p}$	$R_{e,p}$	$f_{e,250}$	$R_{e,250}$	$f_{e,200}$	$R_{e,200}$	$f_{e,150}$	$R_{e,150}$
H0	5.116	0.658	-	-	-	-	-	-
H15-S	17.166	1.249	13.411	0.975	11.727	0.853	9.524	0.693
H15-H	21.032	1.608	12.683	0.970	12.791	0.978	11.951	0.914

As the mid-span deflection increases, the equivalent flexural strength and flexural toughness ratio of both types of steel fiber mixtures decreased, indicating that the load-holding capacity of the specimens was dropping. The deflection corresponding to the peak load of H0 was so small that it showed barely any residual toughness; the post-peak flexural toughness ratio of H15-H tended to drop more slowly than that of H15-S, which indicated a much more stable performance during the failure process. At the last calculating point, the flexural toughness of hooked-end fibers mixtures was 32% greater than that of straight fibers mixtures, while H0 mixtures no longer exhibited toughness performance.

In summary, the test results of toughness of SFRC show that adding fibers to the concrete had a significant change in the compressive failure mode of the concrete. The flexural strengths of the concrete were increased considerably due to the addition of steel fibers. Also, the addition of steel fibers significantly increased the flexural strength of the concrete. As the toughness of SFRC influences the capacity to consume energy, the bond–slip characteristics and corresponding failure modes of tension stiffening of reinforced concrete would also be affected, which would further influence the structural durability and security. Pull-out tests of reinforcement in SFRC would help to study the corresponding influences from the existence of steel fibers in cementitious composites.

3. Bond Test Between SFRC and Reinforcing Bars

Pull-out tests were then carried out to show the embedment length influence on the bond between concrete and reinforcing bars with the hooked-end steel fibers chosen to be mixed in the SFRC.

3.1. Test Specimens, Material Properties and Test Procedures

The specimens are divided into four groups. The dimensional properties for each group are shown in Table 6. Each group has three specimens with the same material and dimensional properties. And hence there are all together 12 specimens of reinforcement embedded in concrete in the experiments. The dimensional properties are as follows. The diameter of reinforcement is 10 mm. All of the specimens have a concrete cover of 30 mm around the reinforcement, which is three times the reinforcement diameter. The specimens are divided into four groups. Group 1 to Group 3 include the reinforcing bars embedded in SFRC. Group 4 as a comparison group includes the reinforcing bars embedded in normal concrete (NC). Group 1 with the specimens named 'SFRC-5d' has an embedment length of 5 times the reinforcing bar diameter, while the embedment length in Group 2 with the specimens named 'SFRC-10d' is 10 times the reinforcing bar diameter. Group 3 has the shortest embedment length, which is 3 times the reinforcing bar diameter, hence resulting in the names of the specimens 'SFRC-3d'. The embedment length of $3d_b$ is to make sure that the pull-out test results directly show the local bond–slip responses instead of the global load–slip responses between reinforcement and the SFRC. Group 4 with the specimens named 'NC-5d' has reinforcement embedded in normal concrete with an embedment length of 50 mm. In addition, the material properties of concrete are depicted in Table 6. The yielding strength of the 10 mm diameter reinforcing bar is 454 MPa, while the ultimate strength is 617 MPa.

Table 6. Dimensional properties of different specimens.

Group No.	Group Name	c (mm)	d_b (mm)	Embedment Length L_e (mm)	Failure Mode
1	SFRC-5d	30	10	5 d_b	Tensile failure
2	SFRC-10d	30	10	10 d_b	Tensile failure
3	SFRC-3d	30	10	3 d_b	Pull-out
4	NC-5d	30	10	5 d_b	Tensile failure

The details of the specimens with reinforcing bars are exhibited in Figure 6. Figure 6a shows the 3-dimensional (3D) schematic diagram of reinforcing bars embedded in the concrete. The middle area is the bonding area between reinforcement and concrete. The bonding area marked as 'nd_b' means it is related to reinforcing bar diameter. The length of the plastic tube at each end is L_{bk}. The plastic tube is anchored in the concrete at each end

to help guarantee the reinforcement anchorage length. Hence, the height for each specimen equals (2 L_{bk} + nd_b). Other parameters in the test are depicted in Figure 6c. The cover 'c' is from the edge of the concrete to the center of the reinforcement. The bar diameter is described as 'd_b'. The cross-section dimension for each specimen is 150 mm × 150 mm, which indicates the 'a' in Figure 6c is 150 mm. The same dimensional details apply to all specimens in tests. The only two differences are (1) the material properties of concrete; and (2) the embedment length of reinforcing bars.
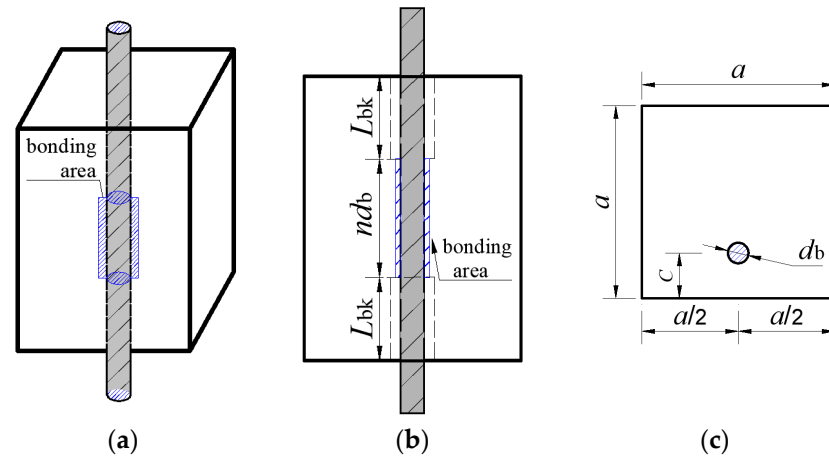

Figure 6. Schematic diagram for specimens in pull-out test. (**a**) Three-dimensional diagram. (**b**) Vertical section. (**c**) Cross-section.

3.2. Test Results and Discussion

The pull-out tests of the reinforcing bars in concrete were then carried out as shown in Figure 7. The specimens were tested with a monotonic load from the Instron machine, as shown in Figure 7a. Then, the load–slip data points were mapped in a computer. The values for the corresponding load and slip were recorded. When the load–slip response was fully developed, the loading procedure would be stopped. When the test for each specimen was finished, the specimen would be removed from the Instron machine. Meanwhile, the failure mode for each specimen was documented through photography.
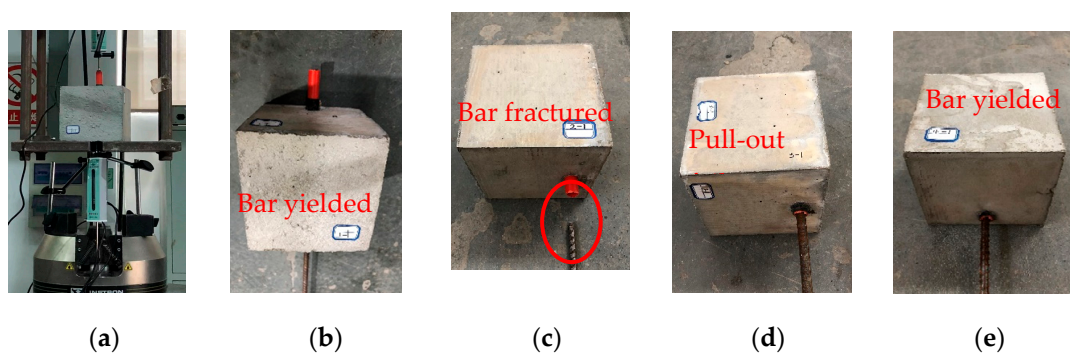

Figure 7. Test setup and corresponding failure modes. (**a**) Test setup. (**b**) Group 1: SFRC-5d. (**c**) Group 2: SFRC-10d. (**d**) Group 3: SFRC-3d. (**e**) Group 4: NC-5d.

Column 6 in Table 6 shows the failure modes for different groups of specimens. It shows that only Group 3 with the embedment length of 3 times the reinforcing bar diameter has the pull-out failure mode while others have the tensile fracture of the reinforcing bars. However, there are slight differences between the tensile fractures of the reinforcing bars. There was slip between the reinforcement and concrete after the reinforcement was yielded in Group 1. And hence the reinforcement was not fractured when the load–slip response

was fully developed. The same phenomenon applies to Group 4. Group 2 has the longest embedment length, which is 10 times the reinforcing bar diameter. The anchorage force guarantees that the capacity of reinforcement could be fully developed. The reinforcing bar fractured after its yielding. In Group 3, there was a very clear descending slope after the ascending branch, which indicates very classic local bond–slip characteristics. The reinforcing bar was pulled out before its yielding, which resulted in the failure mode of pull-out failure instead of tensile failure.

The CT scan work for the concrete blocks was carried out for the SFRC with an embedment length of $5d_b$, $10d_b$, and $3d_b$. The images are shown in Figure 8. The bar was pulled out from the top of the block. For the embedment length of $5d_b$ in Figure 8a, the necking of the reinforcement occurred inside the SFRC block. Compared with SFRC-5d, the specimen of SFRC-10d showed no necking inside the concrete block. However, it could be concluded that for the specimen SFRC-10d, the necking of reinforcement occurred outside of the block illustrated by the failure mode shown in Figure 7c. There was no rebar necking for the SFRC-3d neither inside the concrete block nor outside the block by connecting Figure 8c with Figure 7d. The concrete cracked at the top of the bonding area for both SFRC-5d and SFRC-3d, while there was no obvious crack shown for the SFRC-10d. However, there were gaps between concrete and reinforcement for SFRC-5d, SFRC-10d and SFRC-3d. The differences in the gaps are described as follows. There was a clear gap between the concrete and reinforcement for SFRC-5d and SFRC-3d, showing that there was slip between the concrete and reinforcement along the embedment direction. However, the gap between the concrete and reinforcement for SFRC-10d only accounted for 20% of the bonding area, indicating that there was no slip between the reinforcement and concrete other than that of the 20% of the bonding area.
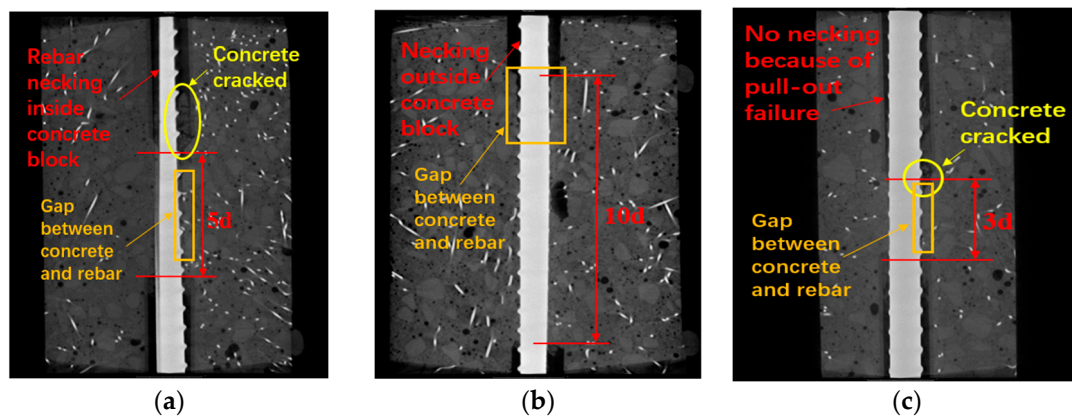

(**a**)   (**b**)   (**c**)

Figure 8. CT scan work of rebar necking, concrete cracking and slip between concrete and rebar. (**a**) Specimen: SFRC-5d. (**b**) Specimen: SFRC-10d. (**c**) Specimen: SFRC-3d.

The load–slip responses for the test specimens were recorded and plotted, as shown in Figure 9. The load–slip responses for each group were obtained by averaging the tested data points from the three specimens in each group. The test results for different groups were compared, as shown in Figure 9a, while the load–slip response for each group are shown in Figure 9b–e, respectively. It shows that for a long embedment length (more than $5d_b$), the peak load in the first arising branch reaches around 33 kN, while the peak load for a short embedment length of $3 d_b$ was 28 kN. This is because for the short anchorage area, the tensile strength of reinforcement was not fully developed. In this stage, the peak load in the arising branch depends on the bond–slip characteristics and the embedment area. When the embedment length reaches a certain value, the anchorage area is large enough to fully develop the tensile capacity of reinforcement, and then the peak load in the arising

branch indicates the yielding capacity of reinforcement. This is the reason for the same peak load values in the ascending stage for Group 1, 2 and 4. Therefore, for the pull-out test of a short embedment length of reinforcement, it gives the local bond–slip characteristics including bond strength. However, for a long embedment length, the test results provide the global load–slip responses, in which case only average bond stress could be calculated.
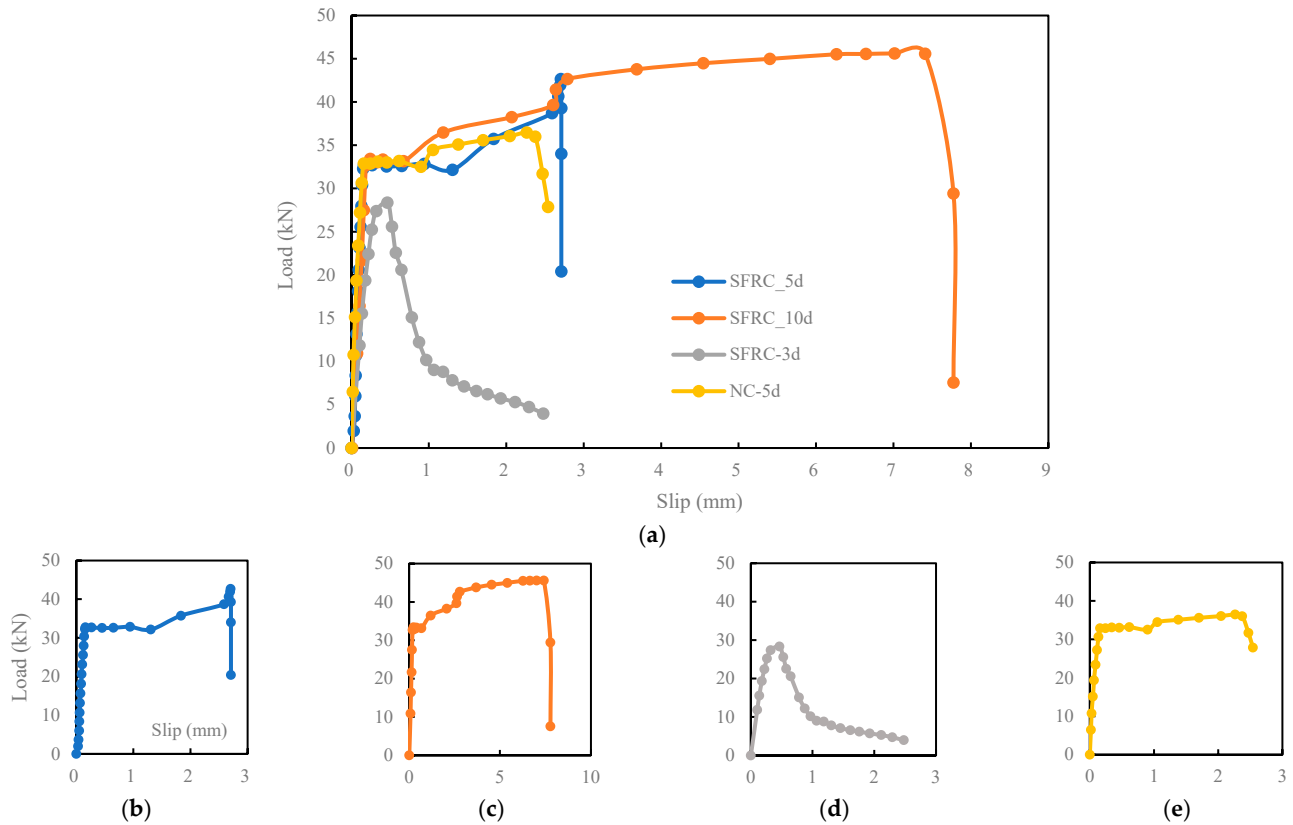

Figure 9. Test results of load–slip responses. (**a**) Load–slip responses for all groups. (**b**) Load–slip responses for SFRC-5d. (**c**) Load–slip responses for SFRC-10d. (**d**) Load–slip responses for SFRC-3d. (**e**) Load–slip responses for NC-5d.

The comparison of load–slip response between Group 1 and Group 4 shows that the fibers in concrete would strengthen the capacity after the yielding plateau of reinforcement. The maximum load in the load–slip response reaches 43 kN in Group 1, while for Group 4, it is 36 kN, with an approximate discrepancy of 18%.

The comparison of results among Groups 1, 2 and 3 indicates the impact of embedment length on the load–slip responses of pull-out of reinforcement in SFRC. The shortest embedment length, which is $3d_b$ in Group 3, gives the local bond–slip characteristics with arising branches and bond strength, which could be obtained from the peak load, descending branch after peak load, and level-off stage when slip reaches a certain value. The longer embedment length, which is $5d_b$ in Group 1, shows a very clear trend of reinforcement yielding. After yielding, the reinforcing bar was pulled out of the SFRC. Comparison of Groups 1 and 2 shows that the load–slip response in Group 1 descends abruptly after the reinforcement reaches its tensile strength, while Group 2 demonstrates a very clear plateau around the tensile strength of reinforcement. It indicates that the longest embedment length of $10d_b$ in Group 2 ensures that the capacity of reinforcement would be fully developed in SFRC.

4. Conclusions

This paper presented experimental investigations of the compressive and flexural toughness of SFRC with two typical steel fiber shapes: the straight steel fiber and the hooked-end steel fiber. The test shows that the concrete with the hooked-end steel fibers exhibits greater toughness than the concrete with the straight steel fiber. In addition, tests on the bond–slip characteristics between the SFRC and the reinforcing bars were also carried out. Different embedment lengths were considered for the influence on the load–slip responses from the pull-out test results. The conclusions are as follows:

(1) Adding fibers to the concrete resulted in a significant change in the compressive failure mode of the concrete but showed little enhancement in the compressive strength. The concrete compressive toughness index shows that the steel fibers had remarkable improvement on the compressive toughness of concrete, and hooked-end steel fibers showed better improvement in the compressive toughness of concrete than straight steel fibers. Also, adding steel fibers improved the ultimate strain of SFRC mixtures. When the compressive strength dropped to 85% of its peak, the strain for specimens with hooked fibers was 1.84 times that of specimens with no fibers and 1.26 times that of specimens with straight fibers.

(2) The flexural strengths of the concrete increased considerably due to the addition of steel fibers. Also, the addition of steel fibers significantly increased the flexural strength of the concrete. The stress–strain curve demonstrated that normal concrete breaks down shortly after the peak point, showing an obvious steep drop tendency. However, both SFRCs (H15-S and H15-H) exhibited deflection about 4 times greater than normal concrete (H0) at their respective peak loads and had relatively complete drop curves, demonstrating ductile behavior.

(3) Tests on the bond–slip characteristics between the reinforcement and SFRC with hooked-end steel fiber were conducted. The test results show that the resisting force between the reinforcement and SFRC is much larger than that between the reinforcement and normal concrete. The critical embedment length between the reinforcement and SFRC is 3 times the bar diameter for the global load–slip responses, showing very clear bond–slip characteristics, while for normal reinforcement concrete, the critical embedment length is 3 times bar diameter, showing a very clear local bond–slip trend.

Author Contributions: H.Z.: Conceptualization, Methodology, Writing—original draft, Writing—Review and Editing, Funding Acquisition; Z.T.: Methodology, Investigation, Formal analysis, Writing—Review and Editing; J.L.: Methodology, Writing—original draft; Z.H.: Formal analysis, Writing—Review and Editing; Q.F.: Conceptualization, Methodology, Investigation, Formal analysis, Visualization, Writing—original draft, Writing—Review and Editing. All authors have read and agreed to the published version of the manuscript.

Data Availability Statement: Data is contained within the article.

Conflicts of Interest: Author Jinguang Li was employed by the company Hunan Track Survey and Design Co., Ltd. The remaining authors declare that the research was conducted in the absence of any commercial or financial relationships that could be construed as a potential conflict of interest.

References

1. Yoo, D.-Y.; Banthia, N. Mechanical properties of ultra-high-performance fiber-reinforced concrete: A review. *Cem. Concr. Compos.* **2016**, *73*, 267–280. [CrossRef]
2. Afroughsabet, V.; Ozbakkaloglu, T. Mechanical and durability properties of high-strength concrete containing steel and polypropylene fibers. *Constr. Build. Mater.* **2015**, *94*, 73–82. [CrossRef]
3. Chajec, A.; Sadowski, Ł. The effect of steel and polypropylene fibers on the properties of horizontally formed concrete. *Materials* **2020**, *13*, 5827. [CrossRef] [PubMed]
4. Nagy, B.; Nehme, S.G.; Szagri, D. Thermal properties and modeling of fiber reinforced concretes. *Energy Procedia* **2015**, *78*, 2742–2747. [CrossRef]
5. Wang, X.; Fan, F.; Lai, J.; Xie, Y. Steel fiber reinforced concrete: A review of its material properties and usage in tunnel lining. *Structures* **2021**, *34*, 1080–1098. [CrossRef]
6. Haktanir, T.; Ari, K.; Altun, F.; Atis, C.D.; Karahan, O. Effects of steel fibers and mineral filler on the water-tightness of concrete pipes. *Cem. Concr. Compos.* **2006**, *28*, 811–816. [CrossRef]
7. Kossakowski, P.G.; Wciślik, W. Fiber-reinforced polymer composites in the construction of bridges: Opportunities, problems and challenges. *Fibers* **2022**, *10*, 37. [CrossRef]
8. Zhang, Y.; Fan, J.; Fan, W. Seismic fragility analysis of concrete bridge piers reinforced by steel fibers. *Adv. Struct. Eng.* **2016**, *19*, 837–848. [CrossRef]
9. Iures, L.; Popa, R.; Bob, C.; Chendes, R. Practical Use of Steel Fibre Reinforced Concretes for Road. In Proceedings of the National Technical-Scientific Conference Modern Technologies for 3rd Millennium, Oradea, Romania, 23–24 March 2017; pp. 169–172.
10. Han, J.; Zhao, M.; Chen, J.; Lan, X. Effects of steel fiber length and coarse aggregate maximum size on mechanical properties of steel fiber reinforced concrete. *Constr. Build. Mater.* **2019**, *209*, 577–591. [CrossRef]
11. Chang, J.; Cui, K.; Zhang, Y. Effect of hybrid steel fibers on the mechanical performances and microstructure of sulphoaluminate cement-based reactive powder concrete. *Constr. Build. Mater.* **2020**, *261*, 120502. [CrossRef]
12. Guo, H.; Jiang, L.; Tao, J.; Chen, Y.; Zheng, Z.; Jia, B. Influence of a hybrid combination of steel and polypropylene fibers on concrete toughness. *Constr. Build. Mater.* **2021**, *275*, 122132. [CrossRef]
13. Bayraktar, O.Y.; Kaplan, G.; Shi, J.; Benli, A.; Bodur, B.; Turkoglu, M. The effect of steel fiber aspect-ratio and content on the fresh, flexural, and mechanical performance of concrete made with recycled fine aggregate. *Constr. Build. Mater.* **2023**, *368*, 130497. [CrossRef]
14. Bae, B.-I.; Chung, J.-H.; Choi, H.-K.; Jung, H.-S.; Choi, C.-S. Experimental study on the cyclic behavior of steel fiber reinforced high strength concrete columns and evaluation of shear strength. *Eng. Struct.* **2018**, *157*, 250–267. [CrossRef]
15. Hung, C.-C.; Hu, F.-Y. Behavior of high-strength concrete slender columns strengthened with steel fibers under concentric axial loading. *Constr. Build. Mater.* **2018**, *175*, 422–433. [CrossRef]
16. Lu, X.; Zhang, Y.; Zhang, H.; Zhang, H.; Xiao, R. Experimental study on seismic performance of steel fiber reinforced high strength concrete composite shear walls with different steel fiber volume fractions. *Eng. Struct.* **2018**, *171*, 247–259. [CrossRef]
17. Zhang, H.; Zhang, Y.; Lu, X.; Duan, Y.; Zhang, H. Influence of axial load ratio on the seismic behavior of steel fiber–reinforced concrete composite shear walls. *J. Struct. Eng.* **2020**, *146*, 04019171. [CrossRef]
18. Koťátková, J.; Reiterman, P. Effects of different types of steel fibers on the mechanical properties of high strength concrete. *Adv. Mater. Res.* **2014**, *1054*, 80–84. [CrossRef]
19. Wu, Z.; Shi, C.; He, W.; Wu, L. Effects of steel fiber content and shape on mechanical properties of ultra high performance concrete. *Constr. Build. Mater.* **2016**, *103*, 8–14. [CrossRef]
20. Kim, J.-J.; Yoo, D.-Y. Effects of fiber shape and distance on the pullout behavior of steel fibers embedded in ultra-high-performance concrete. *Cem. Concr. Compos.* **2019**, *103*, 213–223. [CrossRef]
21. Shaikh, F.U.A. Pullout behavior of hook end steel fibers in geopolymers. *J. Mater. Civ. Eng.* **2019**, *31*, 04019068. [CrossRef]
22. Söylev, T. The effect of fibers on the variation of bond between steel reinforcement and concrete with casting position. *Constr. Build. Mater.* **2011**, *25*, 1736–1746. [CrossRef]
23. Hou, L.; Zhou, B.; Guo, S.; Zhuang, N.; Chen, D. Bond-slip behavior between pre-corroded rebar and steel fiber reinforced concrete. *Constr. Build. Mater.* **2018**, *182*, 637–645. [CrossRef]
24. Wang, L.; Shen, N.; Zhang, M.; Fu, F.; Qian, K. Bond performance of Steel-CFRP bar reinforced coral concrete beams. *Constr. Build. Mater.* **2020**, *245*, 118456. [CrossRef]
25. Dancygier, A.N.; Katz, A.; Wexler, U. Bond between deformed reinforcement and normal and high-strength concrete with and without fibers. *Mater. Struct.* **2010**, *43*, 839–856. [CrossRef]
26. Chao, S.-H.; Naaman, A.E.; Parra-Montesinos, G.J. Bond behavior of reinforcing bars in tensile strain-hardening fiber-reinforced cement composites. *ACI Struct. J.* **2009**, *106*, 897–906. [CrossRef]
27. Sarraz, A.; Nakamura, H.; Kanakubo, T.; Miura, T.; Kobayashi, H. Bond behavior simulation of deformed rebar in fiber-reinforced cementitious composites using three-dimensional meso-scale model. *Cem. Concr. Compos.* **2022**, *131*, 104589. [CrossRef]

28. Hameed, R.; Turatsinze, A.; Duprat, F.; Sellier, A. Bond stress-slip behaviour of steel reinforcing bar embedded in hybrid fiber-reinforced concrete. *KSCE J. Civ. Eng.* **2013**, *17*, 1700–1707. [CrossRef]

29. Yazıcı, S.; Arel, H.S. The effect of steel fiber on the bond between concrete and deformed steel bar in SFRCs. *Constr. Build. Mater.* **2013**, *40*, 299–305. [CrossRef]

30. Soroushian, P.; Mirza, F.; Alhozaimy, A. Bond of confined steel fiber reinforced concrete to deformed bars. *Mater. J.* **1994**, *91*, 141–149.

31. Yan, X.; Shi, Q.; Xu, Z. Experimental study on the bonding performance of steel fibers between concrete and deformed steel reinforcement. *J. Hunan Univ. Nat. Sci. Ed.* **2020**, *1*, 45–52.

32. Gao, D.; Ding, C.; Pang, Y.; Yang, L.; Huang, Y.; Tang, J. Diverse angle-length-width model for 3D/4D/5D steel fiber reinforced concrete under tension. *Constr. Build. Mater.* **2021**, *266*, 121149. [CrossRef]

33. Hajforoush, M.; Kheyroddin, A.; Rezaifar, O.; Kazemi, M. Magnetic ffeld effect on bond performance between reinforcement and concrete containing steel ffbers. *J. Build. Eng.* **2024**, *98*, 111215. [CrossRef]

34. Zhang, H.; Li, H.Y.; Lin, T.X.; Shen, Z.J.; Feng, Q. Experimental investigation on inffuence of embedment length, bar diameter and concrete cover on bond between reinforced bars and steel ffber reinforced concrete (SFRC). *Case Stud. Constr. Mater.* **2024**, *21*, e03742.

35. *CECS19: 2009*; Standard on Test Methods for Fibrous Concrete. China Planning Press: Beijing, China, 2010. (In Chinese)

36. Gao, D.; Zhao, L.; Feng, H.; Zhao, S. Bending toughness of steel fiber concrete and its evaluation method. *J. Constr. Mater.* **2014**, *17*, 7. (In Chinese)